

# Charged pion photoproduction with the $\Delta(1232)$ baryon beyond the resonance region

Seung-il Nam\* and Byung-Geel Yu†

Research Institute for Basic Sciences, Korea Aerospace University, Goyang 412-791, Korea

(Dated: October 30, 2018)

We investigate the charged pion photoproduction off the proton target with the  $\Delta(1232)$  baryon in the final state, i.e.  $\gamma p \rightarrow \pi^- \Delta^{++}(1232)$  and  $\gamma p \rightarrow \pi^+ \Delta^0(1232)$ , based on the effective Lagrangian method, beyond the resonance region,  $E_{\text{cm}} \gtrsim 2$  GeV. We employ the  $\pi$ - and  $\rho$ -meson Regge trajectories in the  $t$ -channel, in addition to the proton- and  $\Delta$ -pole, in the  $s$ - and  $u$ -channels respectively, and the contact-interaction contributions. A specific scheme for the form factor which satisfies the Ward-Takahashi identity, crossing symmetry, and on-shell condition, is taken into account. To discuss the validity of the Regge approach within the Effective Lagrangian method, we also consider a smooth interpolation between the Regge- and Feynman-propagators for the  $t$ -channel meson exchanges as a function of  $\sqrt{s}$ . We present the numerical results for the energy and angular dependences of the cross sections, and double-polarization observable. It turns out that the present framework shows the significance of the  $\pi$ -exchange and contact interaction terms to reproduce the experimental data qualitatively well. Especially, the interpolation between the two propagators plays a crucial role to reproduce the high-energy experimental data. The  $\pi^+$  decay-angle distribution is also studied using the  $\Delta^{++}$ -decay frame, i.e. the Gottfried-Jackson frame. The present results will be a useful guide for future high-energy photon-beam experiments.

PACS numbers: 11.55.Jy, 13.60.Rj, 13.60.Le, 13.85.Fb, 14.20.Gk, 14.40.Be

Keywords:  $\Delta(1232)$  photoproduction, Born approximation, Regge trajectory, Feynman-Regge interpolation

## I. INTRODUCTION

Hadron productions via various scattering processes have been one of the most important experimental and theoretical methods to investigate the strongly-interacting systems, which are governed by the fundamental theory, i.e. *quantum chromodynamics* (QCD), in terms of the color-singlet degrees of freedom. Among the various production processes, photo and electro-productions have been proved to be very useful. Since the photon is a clear probe, these production processes are well suited for investigating hadronic properties, such as the structures, the reaction mechanisms, and so on. Moreover, the nonstrange-meson electro and photoproductions are an extremely good method to investigate the baryon-resonance search. On top of these specific features, according to the gauge-boson nature of the photon, the photocoupling constrains the scattering processes in such a way that the Ward-Takahashi (WT) identity must be satisfied to all orders of Feynman diagrams. Due to this constraint, one can simply identify the necessary Feynman diagrams for a certain scattering process.

Experimentally and theoretically, meson electro and photoproductions have been well studied in various ways. For instance, in the previous work [1], employing the Rarita-Schwinger formalism for spin-3/2 fermions, it turns out that the contact term interaction, which is responsible for conserving the WT identity, plays a dominant role for the  $\Lambda(1520)$  photoproduction. If this is the case, there appears the difference of the production rate between those from the proton and neutron targets related to their isospin structures in each reaction process. Interestingly enough, this theoretical consequence has been confirmed by the experiments [2], and supported theoretically [3]. We also note that the formalism used in Refs. [1, 4, 5] reproduced the presently available data qualitatively very well [5]. Moreover, the recent beam-energy upgrades of the experimental facilities, such as the CLAS12 at Jefferson laboratory [8] and the LEPS2 at SPring-8 [9], may shed light on the measurements for new high-energy data for various photo and electroproduction processes.

In consideration with the success of the theoretical framework employed in Refs. [1, 4, 5] and the present experimental situation mentioned above, we are motivated to investigate the charged pion ( $\pi^\pm$ ) photoproduction off the proton target with  $\Delta(1232, 3/2^+)$  baryon,  $\gamma p \rightarrow \pi^- \Delta^{++}$  and  $\gamma p \rightarrow \pi^+ \Delta^0$ , beyond the resonance region  $E_{\text{cm}} \gtrsim 2$  GeV. Although there are other isospin channels in the final  $\pi\Delta$  state, we would like to focus on these charged pion productions in the present work, because of the abundant experimental data for these specific channels. It is also worth mentioning that these elementary processes are important ingredients to study two pion photoproduction  $\gamma N \rightarrow \pi\pi N$ . As for the

---

\*E-mail: sinam@kau.ac.kr

†E-mail: bgyu@kau.ac.kr

low-energy region, the photo and electroproductions for these elementary-reaction process were already investigated in Refs. [10, 11]. In those works, it turns out that the reaction process contains various contributions, such as those of the Born terms including the nucleon and baryon resonances, the final- (FSI) and initial-state (ISI) interactions, and the Regge poles. However, as will be shown in the later Sections of the present work, only the Born terms and Regge pole contributions almost saturate the reaction process in the high-energy region beyond the resonance region  $E_{\text{cm}} \gtrsim 2$  GeV. In, Ref. [12], the scattering amplitude for  $\gamma N \rightarrow \pi \Delta$  was also parameterized phenomenologically by a simple one-pion exchange. The Regge poles and absorption corrections were employed for the  $\Delta$ -photoproduction in Ref. [13]

As a theoretical framework, as done in Refs. [4, 5], we make use of the effective Lagrangian method and mesonic Regge trajectories. Since we are interested in the energy range beyond the resonance region as mentioned, we will not consider the resonant contributions in the present work for simplicity. Thus, our strategy to investigate the  $\Delta$  photoproduction is quite simple: We take into account the  $\pi$ - and  $\rho$ -meson Regge trajectories in the  $t$  channel for describing the high-energy experimental data, in addition to the tree-level Born terms, such as the the proton- and  $\Delta$ -pole, in the  $s$ - and  $u$ -channels respectively, and contact-term contributions. In treating  $\Delta$  theoretically, we make use of the Rarita-Schwinger vector-spinor formalism [14]. In addition to these ingredients, we also take into account an interpolation between the Feynman and Regge propagators in the  $t$ -channel meson-exchange, considering that the Regge contributions can still affect on the process even in the low energy region. We utilize an ansatz devised for this purpose, which was proved essential to reproduce the low- and high-energy data simultaneously [5]. All the relevant scattering amplitudes are constructed in terms of the tree-level Born approximation without resonant contributions as mentioned. To consider the spatial distributions of the hadrons involved, we introduce the hadron form factors in a gauge-invariant scheme which preserves the Ward-Takahashi identity with the Regge propagators as done in [5, 15].

From the numerical analyses, we will compute the energy and angular dependences of the cross sections, polarization-transfer coefficients, and  $\pi^+$  decay-angle distribution of the process under various conditions. It turns out that unpolarized physical quantities, such as the energy and angular dependences are reproduced qualitatively well beyond the resonance region  $E_{\text{cm}} \gtrsim 2$  GeV as compared to the presently available experimental data. We also discuss the appearance of the strong peak in the forward-scattering region which is decreasing as the photon energy increases. It turns out that this forward peak is generated by the  $t$ -channel pseudoscalar-meson ( $\pi$ ) exchange. The angular dependence  $d\sigma/dt$  shows that the present framework is not enough to reproduce the experimental data for the region, where  $E_\gamma \lesssim 3.5$  GeV and  $-t \gtrsim 0.05$  GeV<sup>2</sup>. Nevertheless the present theoretical framework provides a very good agreement with the experimental data for the high-energy region beyond  $E_\gamma \approx 5$  GeV. Especially, the interpolation of the Feynman and Regge propagators plays an important role to reproduce the data appropriately. From the numerical results for the  $\pi^+$  decay-angle distribution, we find that the contribution of the  $\rho$ -meson exchange is small, but the contact-term contribution and the  $\pi$ -exchange are significant both of which compete with each other in the relatively low energy region. In contrast, only the contact-term contribution dominates the process in the high-energy region.

The present work is structured as follows: In Section II, we briefly explain the theoretical formalism such as the effective Lagrangians for the relevant interactions, gauge-invariant scheme for the form factors, and mesonic Regge trajectories to compute the reaction process which we are interested in. Numerical results and related discussions are given in Section III. We summarize and close with a conclusion in Section IV.

## II. FORMALISMS

In this Section, we explain the theoretical framework for the present calculations for the  $\gamma p \rightarrow \pi \Delta$  reaction process. First, we present the relevant Feynman diagrams for the present reaction process at the tree-level Born approximation in Fig. 1. The four momenta of the particles involved are also given there. We will consider the ( $s, u, t$ )-channel baryon and meson exchanges, and the contact-term contributions. The contact term is necessary for preserving the WT identity of the scattering amplitude as shown in [1]. The interaction Lagrangians for each vertex are defined as follows:

$$\begin{aligned}
\mathcal{L}_{\gamma PP} &= ie_P [(\partial^\mu P^\dagger)P - (\partial^\mu P)P^\dagger] A_\mu, \\
\mathcal{L}_{\gamma PV} &= g_{\gamma PV} \epsilon_{\mu\nu\sigma\rho} (\partial^\mu A^\nu) (\partial^\sigma V^\rho) P + \text{h.c.}, \\
\mathcal{L}_{\gamma NN} &= -\bar{N} \left[ e_N \not{A} - \frac{e\kappa_N}{4M_N} \sigma^{\mu\nu} F_{\mu\nu} \right] N, \\
\mathcal{L}_{\gamma\Delta\Delta} &= -\bar{\Delta}^\mu \left[ \left( F_1 \not{\epsilon} g_{\mu\nu} - F_3 \not{\epsilon} \frac{k_{1\mu} k_{1\nu}}{2M_\Delta^2} \right) - \frac{k_{1\mu} \not{\epsilon}}{2M_\Delta} \left( F_2 g_{\mu\nu} - F_4 \frac{k_{1\mu} k_{1\nu}}{2M_\Delta^2} \right) \right] \Delta^\nu, \\
\mathcal{L}_{PN\Delta} &= \frac{g_{PN\Delta}}{M_P} \bar{\Delta}^\mu \partial_\mu P N + \text{h.c.},
\end{aligned}$$

$$\begin{aligned}
\mathcal{L}_{VN\Delta} &= -\frac{ig_{VN\Delta}^{(1)}}{m_V}\bar{\Delta}^\mu\gamma^\nu\gamma_5V_{\mu\nu}N - \frac{g_{VN\Delta}^{(2)}}{m_V^2}\bar{\Delta}^\mu\gamma_5V_{\mu\nu}\partial^\nu N + \frac{g_{VN\Delta}^{(3)}}{m_V^2}\bar{\Delta}^\mu\partial^\nu\gamma_5V_{\mu\nu}N + \text{h.c.}, \\
\mathcal{L}_{\gamma PN\Delta} &= -\frac{ie_N g_{PN\Delta}}{M_P}\bar{\Delta}^\mu A_\mu PN + \text{h.c.},
\end{aligned} \tag{1}$$

where  $e_h$  stands for the electric charge of the hadron  $h$ , whereas  $e$  is the unit electric charge.  $A$ ,  $P$ ,  $V$ ,  $N$ , and  $\Delta$  denote the fields for the photon, pseudoscalar and vector mesons, nucleon, and  $\Delta$ , respectively. The magnetic moment of the proton is  $2.79\mu_N$ , giving  $\kappa_p = 1.79$  for the present case [16]. The antisymmetric tensor is defined by  $\sigma = i(\gamma_\mu\gamma_\nu - \gamma_\nu\gamma_\mu)/2$ , and the  $F_{\mu\nu}$  and  $V_{\mu\nu}$  are the field-strength tensors for the photon and vector meson, respectively. Note that  $F_{1\sim 4}$  are the multipole moments of the  $\Delta$ , corresponding to the monopole, dipole, quadrupole, and octupole ones. Since there are no experimental and theoretical information for the  $F_3$  and  $F_4$ , we will ignore them for brevity in the numerical calculations. As for  $\Delta^{++}$ , we have  $F_1 = e_\Delta$  and  $F_2 = \mu_{\Delta^{++}} = (3.7 \sim 8.5)\mu_N$  from the average value of the experimental data [16]. From the theoretical calculations, such as the model-independent way of the chiral quark soliton model ( $\chi$ QSM) [17, 18] and the SU(6) quark model [19], it was estimated as  $(5.34 \sim 5.40)\mu_N$  and  $5.58\mu_N$ , respectively. Hence, the middle value from Ref. [16],  $5.6\mu_N$  must be a reasonable choice for numerical calculations, which leads to  $\kappa_{\Delta^{++}} = 3.6$ . As for the neutral  $\Delta$ , we employ  $\kappa_{\Delta^0} = -0.063$  [16]. The coupling strength of  $g_{\pi N\Delta}$  can be computed from the experimental data of its full decay width  $\Gamma_{\Delta \rightarrow \pi N} = (116 \sim 120)$  MeV with  $\Gamma_\Delta/\Gamma_{\Delta \rightarrow \pi N} \approx 100\%$  [20]. By using the Yukawa vertex, defined by  $\mathcal{L}_{PN\Delta}$  in Eq. (1), we obtain the following relation [21]:

$$\Gamma_{\Delta \rightarrow \pi N} = \frac{1}{6} \left[ \frac{(M_\Delta + M_N)^2 - m_\pi^2}{M_\Delta^2} \right] \frac{g_{\pi N\Delta}^2 |\mathbf{p}_{\pi N}|^3}{4\pi m_\pi^2}, \tag{2}$$

where  $\mathbf{p}_{\pi N}$  indicates the three momentum of the decaying particle which can be easily calculated by the Källén function [20]:

$$\mathbf{p}_{\pi N} = \frac{\sqrt{[M_\Delta^2 - (M_P + M_N)^2][M_\Delta^2 - (M_P - M_N)^2]}}{2M_\Delta} \approx 227 \text{ MeV}. \tag{3}$$

Substituting the experimental information,  $m_\pi \approx 138$  MeV,  $M_N \approx 939$  MeV, and  $M_\Delta \approx 1232$  MeV, into Eq. (2) and using Eq. (3), one is led to  $g_{\pi N\Delta} \approx (2.14 \sim 2.18)$ . In numerical calculations, we will make use of  $g_{PN\Delta} = 2.16$  as a trial. As for the  $\rho$ -meson exchange, the value of  $g_{\gamma\pi\rho}$  can be estimated by using the interaction Lagrangian in Eq. (1) for the experimental data  $\Gamma_{\rho^\pm \rightarrow \gamma\pi^\pm} \approx 68.59$  keV, and we have it as  $0.245/\text{GeV}$  for the charged decay. The  $g_{VN\Delta}^{(1,2,3)}$  stand for the relevant strong coupling strengths at the vector-nucleon- $\Delta$  vertex. Again, taking into account the limited information on these couplings, we will set them zero as a trial, except for  $g_{VN\Delta}^{(1)} \equiv g_{\rho N\Delta}$ . Using a mesonic model, the value of  $g_{\rho N\Delta}$  was determined as  $(3.5 \sim 7.8)$  from Ref. [22] and references therein. We will use the average value for it,  $g_{\rho N\Delta} = 5.65$  for the numerical calculations.

Using the interaction Lagrangians defined in Eq. (1) for the  $\gamma p \rightarrow \pi^- \Delta^{++}$  and  $\gamma p \rightarrow \pi^+ \Delta^0$  reaction process, we construct the gauge invariant amplitudes for the  $s$ -,  $u$ -, and  $t$ -channel contributions:

$$\begin{aligned}
i\mathcal{M}_s &= \frac{g_{\pi N\Delta}}{M_\pi} \bar{u}_\mu k_2^\mu \left[ \frac{e_N \left[ \not{k}_1 F_s + (\not{p}_1 + M_N) \hat{F} \right]}{s - M_N^2} + \frac{e\kappa_N}{2M_N} \frac{(\not{k}_1 + \not{p}_1 + M_N) F_s \not{k}_1}{s - M_N^2} \right] \not{\epsilon} u, \\
i\mathcal{M}_u &= \frac{g_{\pi N\Delta}}{M_\pi} \bar{u}_\mu \not{\epsilon} \left[ \frac{e_\Delta \left[ (\not{p}_2 + M_\Delta) \hat{F} - \not{k}_1 F_u \right]}{u - M_\Delta^2} + \frac{e\kappa_\Delta}{2M_\Delta} \frac{\not{k}_1 (\not{p}_2 - \not{k}_1 + M_\Delta) F_u}{u - M_\Delta^2} \right] G^{\mu\nu} k_{2\nu} u, \\
i\mathcal{M}_c &= -\frac{e_\pi g_{\pi N\Delta}}{M_\pi} \hat{F} \bar{u}_\mu \epsilon^\mu u, \\
i\mathcal{M}_{t(\pi)} &= -\frac{2e_\pi g_{\pi N\Delta}}{M_\pi} \hat{F} \bar{u}_\mu (k_1^\mu - k_2^\mu) (k_2 \cdot \epsilon) u \mathcal{D}_\pi, \\
i\mathcal{M}_{t(\rho)} &= \frac{ig_{\gamma\pi\rho} g_{\rho N\Delta}}{M_\rho} F_t \bar{u}_2^\mu \gamma_\nu \left[ (k_1^\mu - k_2^\mu) g^{\nu\sigma} - (k_1^\nu - k_2^\nu) g^{\mu\sigma} \right] (\epsilon_{\rho\eta\xi\sigma} k_1^\rho \epsilon^\eta k_2^\xi) \gamma_5 u_1 \mathcal{D}_\rho,
\end{aligned} \tag{4}$$

where  $k_1$ ,  $k_2$ ,  $p_1$ , and  $p_2$  are the momenta of the incident photon, outgoing pion, target proton, and recoiled  $\Delta$ .  $\mathcal{D}_{\pi,\rho} = 1/(t - M_{\pi,\rho}^2)$  are the  $t$ -channel  $\pi$  and  $\rho$ -meson propagators, respectively.  $F_{s,u,t}$  stand for the phenomenological hadronic form factors to consider the spatial distributions of the relevant hadrons:

$$F_x = \frac{\Lambda^4}{\Lambda^4 + (x - M_x^2)^2}, \tag{5}$$

where the subscript  $x$  stands for the Mandelstam variables and  $M_x$  the mass of the off-shell hadron in the  $x$  channel [23–25]. The cutoff mass  $\Lambda$  will be determined to reproduce the experimental data in the next Section.  $G_{\mu\nu}$  denotes the projection operator for the spin-3/2 fermion, assigned as

$$G_{\mu\nu} = g_{\mu\nu} - \frac{1}{3}\gamma_\mu\gamma_\nu - \frac{2}{3M_\Delta^2}q_\mu q_\nu + \frac{q_\mu\gamma_\nu - q_\nu\gamma_\mu}{3M_\Delta}, \quad q = p_2 - k_1. \quad (6)$$

Although the spin-3/2 projector is defined as above, we will simplify it by setting  $G_{\mu\nu} \approx g_{\mu\nu}$ , which is verified that no significant distinction is observed by this simplification as long as we are interested in the two-body final-state reaction process. Following the prescription suggested and employed in Refs. [1, 4, 5, 23–25], we employ an overall form-factor  $\hat{F}$  to maintain the WT identity of the scattering amplitude,

$$\hat{F} = 1 - (1 - F_s)(1 - F_t)(1 - F_u). \quad (7)$$

We note that this form-factor scheme preserves the gauge invariance, crossing symmetry, and on-shell condition of the form factors, simultaneously. The electric charges in Eq. (4) are assigned as  $(e_\pi, e_N, e_\Delta) = (-e, +e, +2e)$  and  $(+e, +e, 0)$  for the  $\pi^-$  and  $\pi^+$  photoproductions, respectively, to satisfy the electric-charge conservation.

As mentioned previously, since we are interested in the region beyond that of the resonances, it is necessary to take into account a method to go over the Born approximation which is believed to be reliable only for the low energy region. As in Ref. [5–7, 26, 27], the prescription of the Regge-trajectory for the  $t$ -channel meson pole is one of the most successful and practical method for this purpose. As for the case of the  $\gamma p \rightarrow K^+\Lambda(1520)$  photoproduction [5], where threshold energy is about  $E_\gamma \approx 1.67$  GeV, the Regge contribution becomes significant beyond  $E_\gamma \approx 4$  GeV. Furthermore, the Regge contribution turns out to be responsible for reproducing the angular dependence of the scattering process correctly, especially for the momentum-transfer  $t$  dependence, i.e.  $d\sigma/dt$  in the high-energy region.

In the present work, we will consider the Regge trajectories for the pion and rho meson in the  $t$ -channel. However, for simplicity, we will not consider the axial-vector and tensor mesons, such as the  $a_1(1260, 1^+)$ ,  $b_1(1235, 1^+)$ , and  $a_2(1320, 2^+)$ , and so on. As discussed in Refs. [5, 6], the prescription for the Reggeization can be applied to the present framework by replacing the  $t$ -channel Feynman propagators in the invariant amplitudes in Eq. (4) with the following one:

$$\mathcal{P}_X = \frac{\pi\alpha'_X}{\Gamma[\alpha_X(t) - J_X + 1] \sin[\pi\alpha_X(t)]} \left(\frac{s}{s_0}\right)^{\alpha_X(t) - J_X}, \quad \alpha_X(t) = J_X + \alpha'_X(t - m_X^2)\text{GeV}^{-2}, \quad (8)$$

where  $\alpha_X$  denotes the Regge trajectory for the meson  $X$  as a function of  $t$  with the slope  $\alpha'_X$ .  $J_X$  and  $m_X$  stand for the spin and mass of the meson, respectively. Here is a caveat; in deriving Eq. (8), all the even and odd spin trajectories are assumed to be degenerate, although in reality these trajectories are not degenerated [6, 7, 28, 29]. Moreover, for convenience, we have set the phase factor for the propagators to be positive unity as done in Ref. [15]. The cutoff parameter  $s_0$  is chosen to be 1 GeV conventionally [6, 7, 27]. Since the  $\Gamma$  function in Eq.(8) plays the role of the form factor in the Feynman propagator to suppress the divergence of the Regge propagator at the singularities  $\sin[\pi\alpha_X(t)] = 0$ , we will not consider the form factors given in Eq. (4), setting all of them to unity for the Regge-trajectory calculations. Hereafter, we use a notation  $i\mathcal{M}^{\text{Regge}}$  for the amplitude constructed with the Regge propagators in Eq. (8). We list the relevant inputs for the Regge trajectories in Table I.

	$J^P$	$m_X$	$J_X$	$\alpha'_X$
$\pi$	$0^-$	140 MeV	0	0.7
$\rho$	$1^-$	770 MeV	1	0.8

TABLE I: Relevant inputs for the Regge trajectory of the meson  $X$ .

Let us now discuss the gauge invariance of the present invariant amplitude where the  $\pi$  and  $\rho$  exchanges in Eq. (4) are Reggeized with the Regge propagators in Eq. (8). Following the procedure in Refs. [6, 7, 27–29] for the  $t$ -channel Reggeization, we write the Reggeized amplitude for the  $\pi$  exchange as

$$i\mathcal{M} = i\mathcal{M}_{t(\pi,\rho)}^{\text{Regge}} + (i\mathcal{M}_s + i\mathcal{M}_u + i\mathcal{M}_c). \quad (9)$$

It is, then, easy to show that the amplitude in Eq. (9) does not satisfy the current conservation (WT identity) as follows:

$$k_1 \cdot (i\mathcal{M}) = k_1 \cdot (i\mathcal{M}_{t(\pi)}^{\text{Regge}} + i\mathcal{M}_s^E + i\mathcal{M}_u^E + i\mathcal{M}_c) \neq 0. \quad (10)$$

Hence, the sum of the  $\pi$ -exchange in the  $t$ -channel and electric  $s$ - and  $u$ -channel contributions must be zero to satisfy the gauge invariance, whereas the  $\rho$ -exchange and magnetic contributions are automatically zero, due to their antisymmetric nature. To satisfy the gauge invariance, we follow the prescription, suggested in Refs. [6, 7, 27–29] as

$$i\mathcal{M}_{t(\pi)}^{\text{Regge}} + i\mathcal{M}_s^E + i\mathcal{M}_u^E + i\mathcal{M}_c \rightarrow i\mathcal{M}_{t(\pi)}^{\text{Regge}} + (i\mathcal{M}_s^E + i\mathcal{M}_u^E + i\mathcal{M}_c)(t - m_\pi^2)\mathcal{P}_\pi \equiv i\bar{\mathcal{M}}^{\text{Regge}}, \quad (11)$$

where we set  $F_{s,u}$  and  $\hat{F}$  to be unity for the  $i\bar{\mathcal{M}}^{\text{Regge}}$ . Thus, the Reggeized amplitude can be written as follows:

$$i\mathcal{M} = i\bar{\mathcal{M}}^{\text{Regge}} + i\mathcal{M}_s^M + i\mathcal{M}_u^M + i\mathcal{M}_{t(\rho)}^{\text{Regge}}, \quad (12)$$

where the superscript  $M$  denotes the magnetic contributions of the  $s$  and  $u$  channels.

We recall that the Regge propagators should work properly for the energy and momentum transfer  $(s, |t|) \rightarrow (\infty, 0)$ , but in practice the Regge contributions could nevertheless affect even in the low-energy region  $(s, |t|) \rightarrow (s_{\text{threshold}}, \text{finite})$ . Thus, it is physically reasonable to suppose that the meson propagators are smoothly shifted from the Regge one at high energy for  $s \gtrsim s_{\text{Regge}}$  to the usual Feynman one in the low energy for  $s \lesssim s_{\text{Regge}}$ . Here,  $s_{\text{Regge}}$  indicates a certain value of  $s$  from which the Regge contributions become effective. As discussed in Ref. [5] in detail, there is no unique scheme to interpolate these two regions. Thus, as a trial, we introduce to the relevant invariant amplitudes in Eq. (4) an ansatz which interpolates between the Feynman and Regge realms by redefining the form factors as follows:

$$\hat{F} \rightarrow \bar{F}_c \equiv [(t - M_X^2)\mathcal{P}_X] \mathcal{R} + \hat{F}(1 - \mathcal{R}), \quad (13)$$

where the ansatz for the interpolation reads

$$\mathcal{R} = \frac{1}{2} \left[ \tanh \left( \frac{s - s_{\text{Regge}}}{s'} \right) + 1 \right]. \quad (14)$$

Here,  $s'$  denotes a free parameter to make the argument of  $\tanh$  in Eq. (14) dimensionless. It is easy to understand that  $\mathcal{R}$  goes to unity as  $s \rightarrow \infty$  and approaches to zero as  $s \rightarrow 0$ . This asymptotic behaviors of  $\mathcal{R}$  ensures that  $\bar{F}_c$  in Eq. (13) interpolates the two energy regions smoothly. As already shown in Ref. [5], this interpolation could describe qualitatively very well the low- and high-energy region data, simultaneously. We will determine the parameters,  $s_{\text{Regge}}$  and  $s'$ , with experimental data in the next Section. We want to indicate the difference of the interpolation function in the present work from that in Ref. [5] briefly. In the previous work, there was an additional term which was multiplied to Eq. (14) as a function of  $t$ , as we considered the  $t$  dependence of the Regge trajectories. However, since we verified that it is not effective for a considerably wide energy range we will ignore such a  $t$ -dependent term here, and as a result, we have the interpolation function as a function of  $s$  as in Eq. (14). Consequently, as discussed above, we will have three distinctive models in the following Sections, assigned as:

1. *Born*: The scattering amplitude is defined with the conventional Feynman propagators with the phenomenological form factors as in Eqs. (4), (5), and (7).
2. *Regge*: The scattering amplitude is modified by the Regge contributions without form factors as in Eq. (12).
3. *Interpolation*: The *Regge* approach is modified by the interpolation formula and ansatz in Eqs. (13) and (14).

### III. NUMERICAL RESULTS AND DISCUSSIONS

In this Section, we present the numerical results for the various physical observables such as the energy and angular dependences of the cross sections for the two charged pion photoproduction processes. We also show the numerical results for the polarization-transfer coefficient ( $C_{x,z}$ ) [4, 30, 31] and the  $\pi^+$ -decay angle distribution [5, 32] for the two production processes. The results are compared with experimental data, and we provide theoretical estimations useful for future experiments.

First, we investigate the unpolarized total cross section as a function of the photon energy  $E_\gamma$  in the three different models. We present the results for the  $\pi^-$  photoproduction in the left panel of Fig. 2 in which the solid, dotted, and dot-dashed lines correspond to the Born, Regge, and interpolation models, respectively. The experimental data are taken from Refs. [33–35]. All the calculations are performed with the cutoff mass  $\Lambda \approx 450$  MeV, determined to reproduce the data. Note that this cutoff mass is about 25% smaller than that for the  $\Lambda(1520)$  photoproduction [1, 4, 5]. The simple Born model provides qualitatively good agreement with the data, whereas the Regge one corresponding to  $\mathcal{R} = 1$  shows overshoot in the lower energy region. This observation indicates that the simple replacement of the

$t$ -channel Feynman propagators with the Regge ones in the present case does not work so well. In the application of the interpolation ansatz with the relevant parameters determined as  $s_{\text{Regge}} = (3.5 \text{ GeV})^2$  and  $s' = (2.5 \text{ GeV})^2$ , we obtain a reasonable result as shown in Fig. 2. These values indicate that the Regge contribution starts to dominate the present reaction process beyond  $\sqrt{s} \approx 3.5 \text{ GeV}$ . As for the  $\pi^+$  photoproduction, it turns out that one needs much smaller cutoff mass to reproduce the experimental data qualitatively, i.e.  $\Lambda \approx 200 \text{ MeV}$  as shown in the right panel of Fig. 2 for the Born and interpolation models. Note that this cutoff value is much smaller than that for the  $\pi^-$  photoproduction, signaling that there can be considerable contributions from those beyond the ground-state nucleon, for instance. The numerical results for the Born and interpolation models show similar energy dependence, whereas their strengths are rather different, although the experimental data contain sizable uncertainties in this channel. Note that the Regge-model result strongly overshoots the data which are not depicted here.

The left panel of Fig. 3 shows the differential cross section for the  $\pi^-$  photoproduction as a function of  $E_\gamma$  for the three different angles,  $\theta = (0, 30^\circ, 60^\circ)$  with the same legends for the lines with those in Fig. 2. At the very forward angle  $\theta = 0$ , the strength of the cross section decreases monotonically for the three cases without showing significant differences. On the contrary, as the angle increases, the difference between them becomes obvious, according to the considerable contributions from the Regge trajectories. The difference between the models with and without the interpolation turns out to be moderate for  $\theta \gtrsim 30^\circ$ , and becomes negligible at  $\theta = 60^\circ$ .

In the right panel of Fig. 3, we draw the differential cross section as a function of  $\theta$  for different energies,  $E_\gamma = (2, 6, 10) \text{ GeV}$ , presented in the same manner with the left panel. From this we can conclude that there is the strong  $t$ -channel contribution, which makes a peak in the forward scattering region. This tendency is rather different from that of the  $\Lambda(1520)$  photoproduction, in which case the contact-term contribution dominates the reaction process [1, 4, 5]. As the energy increases, the overall strength of the differential cross sections become smaller and the peak position moves to the vicinity around  $\theta = 0$ . We will discuss the shift of the peak-position in detail below. We note that the Born and interpolation models provide almost negligible contributions in the backward scattering region,  $\theta \gtrsim 60^\circ$ , which can be understood easily from the left panel of Fig. 3: the smaller strengths for the larger angles.

Now, we are in a position to discuss the momentum-transfer dependence of the present reaction process, represented by  $d\sigma/dt$  as a function of  $-t$  in Fig. 4. The three cases for the Born (A), Regge (B), and interpolation (C) models are presented separately for the four different energy ranges,  $E_\gamma = (2.4 \sim 2.8) \text{ GeV}$ ,  $(2.8 \sim 3.6) \text{ GeV}$ ,  $(3.6 \sim 4.4) \text{ GeV}$ , and,  $(4.4 \sim 4.8) \text{ GeV}$ , in which the shaded band stands for each energy interval. The experimental data are taken from Ref. [36]. As for the Born model (A) in Fig. 4, the experimental data are qualitatively well reproduced in the region  $-t = (0.05 \sim 0.2) \text{ GeV}^2$ . Outside that region, only the high energy data around  $E_\gamma \approx 4.6 \text{ GeV}$  are relatively in good agreement with the theoretical prediction. In other words, these observations tell us that there can be missing contributions for the lower energy region in the present framework, especially for the small  $|t|$  region. Such discrepancies indicate that one may need to consider further contributions from the  $N$  and  $\Delta$  resonances around  $E_{\text{cm}} = (2 \sim 3) \text{ GeV}$  and possibly from other kinds of  $t$ -channel meson exchanges, which we are not considering here. As we take into account the Regge contributions as shown in the panel B, there appears strong enhancement for the region beyond  $-t \gtrsim 0.2 \text{ GeV}^2$ , which overshoots the data. Again, this unexpected overestimation is tamed by including the interpolating ansatz as seen in the panel C of Fig. 4, which leads to relatively a good agreement with the experimental data. In the panel D, we draw each contribution separately for the  $d\sigma/dt$  at  $E_\gamma = 2.4 \text{ GeV}$ , using the Born model, in order to see which contribution is essential to produce the curve. As shown there, the  $\pi$ -exchange and contact-term contribution dominate the forward scattering region, whereas the others are considerably small. Moreover, one can easily see that the contact-term contribution makes the peak shifted to the smaller  $t$  region ( $-t \approx 0.01 \text{ GeV}^2$ ). By comparing this observation with the right panel of Fig. 3 and seeing the shift of the peak, one can easily find that the contact-term contribution gets prevailing over the  $\pi$ -exchange as  $E_\gamma$  increases, although the contribution of the  $\pi$ -exchange is still dominant. In the panel E of Fig. 5, we also show the numerical results, using the interpolation model, for the  $\pi^+$  photoproduction. Again, we observe similar tendency with that for the  $\pi^-$  one.

In Fig. 6, we present the numerical results of the momentum-transfer dependence,  $d\sigma/dt$  for the higher photon-energy regions,  $E_\gamma = 5$  (A), 8 (B), 11 (C), and 16 (D) GeV. The experimental data are taken from Refs. [37–39]. Similarly, we draw the three models, the Born (solid), Regge (dot), and interpolation (dash), separately. It can be clearly seen that the interpolation model yields considerably excellent results in comparison with the experimental data. We also find that the results from the Born approximation are only reliable below  $-t \approx 0.1 \text{ GeV}^2$  for all the photon energies. Beyond this value, we observe that the Regge contribution plays a critical role as shown in the panels of Fig. 6. At the same time, the interpolation ansatz works very well for these relatively high energy ranges. For instance, we see that the value of  $\mathcal{R}$  becomes about 0.4, which indicates that the contributions from the Regge and Feynman propagators are almost in the same portion, for  $E_\gamma = 5 \text{ GeV}$ . As expected, much higher energy such as  $E_\gamma = 16 \text{ GeV}$ , the  $\mathcal{R}$  becomes almost unity, i.e. the Regge propagator prevails almost completely over the Feynman one. As for the  $\pi^+$  photoproduction, we again find a qualitative agreement with the data as shown in the panel E of Fig. 7, although sizable deviation observed in comparison to that for the  $\pi^-$  one. Hereafter, we will show the numerical results only from the interpolation model, since we have proven that it has reproduced the experimental

data qualitatively well so far.

Now, we want to discuss the polarization physical quantities especially for the  $\pi^-$  photoproduction, such as the polarization-transfer coefficients  $C_{x,z}$  and related pion-decay distribution. Among the polarization observables in a meson photoproduction,  $C_x$  and  $C_z$  are identified as the spin asymmetry along the direction of the polarization of the recoil baryon with the circularly polarized photon beam. First, we define the polarization transfer coefficients in the  $(x', y', z')$ -coordinate, being similar to those for the spin-1/2 hyperon-photoproduction as in Refs. [30, 31]:

$$C_{x',|S_{x'}|} = \frac{\frac{d\sigma}{d\Omega}_{r,0,+S_{x'}} - \frac{d\sigma}{d\Omega}_{r,0,-S_{x'}}}{\frac{d\sigma}{d\Omega}_{r,0,+S_{x'}} + \frac{d\sigma}{d\Omega}_{r,0,-S_{x'}}}, \quad C_{z',|S_{z'}|} = \frac{\frac{d\sigma}{d\Omega}_{r,0,+S_{z'}} - \frac{d\sigma}{d\Omega}_{r,0,-S_{z'}}}{\frac{d\sigma}{d\Omega}_{r,0,+S_{z'}} + \frac{d\sigma}{d\Omega}_{r,0,-S_{z'}}}, \quad (15)$$

where the subscripts  $r$ ,  $0$ , and  $\pm S_{x',z'}$  stand for the right-handed photon polarization, unpolarized target nucleon, and polarization of the recoil baryon along the  $x'$ - or  $z'$ -axis, respectively. Since the photon helicity is fixed to be +1 here,  $C_{x'}$  and  $C_{z'}$  measures the polarization transfer to the recoil baryon. Moreover,  $C_{x'}$  and  $C_{z'}$  behave as the components of a three vector so that it can be rotated to the  $(x, y, z)$ -coordinate as:

$$\begin{pmatrix} C_x \\ C_z \end{pmatrix} = \begin{pmatrix} \cos\theta_K & \sin\theta_K \\ -\sin\theta_K & \cos\theta_K \end{pmatrix} \begin{pmatrix} C_{x'} \\ C_{z'} \end{pmatrix}, \quad (16)$$

where the  $(x, y, z)$ -coordinate stands for that the incident photon momentum is aligned to the  $z$ -axis. These polarization quantities were already investigated for the spin-1/2 [31] and spin-3/2 [4, 5] baryons. The numerical results for  $C_{x,z}$  are presented in Fig. 8, employing the interpolation mode only, for different  $E_\gamma$  values. All the results show  $C_z = 1$  and  $C_x = 0$  in the collinear limit, i.e. at  $\cos\theta = \pm 1$ , due to the helicity conservation. Generally, we observe very complicated structures for the vicinity  $\cos\theta \gtrsim 0.5$ , since there happen complicated interferences between the  $\pi$ -exchange and contact-term contributions. For  $E_\gamma \gtrsim 8$  GeV, the shapes of the curves remain relatively unchanged. This tendency, negligible changes for the higher photon energies, was already observed for the  $\Lambda(1520)$  photoproduction [4, 5]. We expect that these  $C_{x,z}$  for the  $\Delta$  photoproduction at high energy can be measured by CLAS collaboration Jefferson laboratory, considering their upgrading photon-beam energy and high performance of the circular photon polarization, as already done for the ground state  $\Lambda$  hyperon, i.e.  $\Lambda(1192)$  [30].

Our last topic is the  $\pi^+$  decay-angle distribution function for the  $\pi^-$  photoproduction process. The decay-angle distribution has been already discussed experimentally for the  $\Lambda(1520)$  photoproduction [32, 42]. Theoretically, it was also explored in the previous work [4, 5]. The decay-angle distribution is the angle distribution of  $\pi^+$  that decays via  $\Delta^{++} \rightarrow \pi^+ p$  in the  $t$ -channel helicity frame, i.e. the Gottfried-Jackson frame [43]. Schematic figures for this frame and kinematics are shown in Fig. 9, in which the decay angle  $\phi$  is defined. From this distribution function one can see which meson-exchange is dominating the production process. According to the spin statistics, the distribution function becomes proportional to  $\sin^2\phi$  for  $\Delta^{++}$  in  $S_z = \pm 3/2$ , whereas  $\frac{1}{3} + \cos^2\phi$  for  $\Delta^{++}$  in  $S_z = \pm 1/2$ . As in Ref. [42, 44], considering all the possible contributions, we can parametrize the distribution function as follows:

$$\mathcal{F}_{\pi^+} = A \sin^2\phi + B \left( \frac{1}{3} + \cos^2\phi \right), \quad (17)$$

where we have used a notation  $\mathcal{F}_{\pi^+}$  indicating the distribution function for convenience. The coefficients  $A$  and  $B$  stand for the strength of each spin state of  $\Delta^{++}$  with the normalization condition  $A + B = 1$ . In other words, if  $A > B$ , one can think that the spin-1 particle exchange or an equivalent contribution in the  $t$  channel dominates the scattering process, and vice versa for the spin-0 particle exchange. We note that there can be other hyperon contributions beside  $\Delta^{++}$  so that one can add an additional term to Eq. (17) representing the interference effects. However, we will ignore it for simplicity as done in Refs. [4, 5].

Now, we want to provide theoretical estimations on  $\mathcal{F}_{\pi^+}$ . Note that we again only show the numerical results for the interpolation model hereafter. Since the outgoing pion ( $\pi^-$ ) carry no spin, all the photon helicity will be transferred to  $\Delta^{++}$  through the exchanging particle in  $t$ -channel, Hence, it is natural to think that the polarization-transfer coefficients in the  $z$  direction should relate to the strength coefficients  $A$  and  $B$ . Therefore, we can write  $A$  and  $B$  in terms of  $C_{z,1/2}$  and  $C_{z,3/2}$  as follows:

$$A = \frac{C_{z,3/2}}{C_{z,1/2} + C_{z,3/2}}, \quad B = \frac{C_{z,1/2}}{C_{z,1/2} + C_{z,3/2}}, \quad (18)$$

which satisfy the normalization condition. In other words,  $A$  denotes the strength that  $\Delta^{++}$  is in its  $S_z = \pm 3/2$  state, and  $B$  for  $S_z = \pm 1/2$ . In Fig. 10, we depict the distribution as a function of  $\phi$  for different  $\theta = (10 \sim 50)^\circ$  and  $E_\gamma = (3, 9)$  GeV. As for the lower energy ( $E_\gamma = 3$  GeV), the numerical results tell us that the scattering process is

mainly dominated by the spin-1 exchange or equivalent contribution for the very forward scattering angles. Moreover, this observation indicates that the contact-term contribution dominates the process, since it can be interpreted equivalently as a spin-1 exchange, and the contact-term one is much more effective than that of the  $\rho$ -exchange as discussed above. However, for the angle around  $\theta = 30^\circ$ , the spin-0 exchange, i.e.  $\pi$ -meson exchange, contributes significantly, denoted by the short-dash line in the left panel of Fig. 10. Beyond that angle, again, the contact-term contribution prevails over that from the spin-0 one. As for the higher energy region, the situation becomes quite different from the lower energy case. In the right panel of Fig. 10, we show the decay-angle distribution for  $E_\gamma = 9$  GeV. We see that, for all the  $\pi^-$  angles, the contact-term contribution dominates the process, in addition to the tiny  $\rho$ -meson exchange one, as understood from the panel D in Fig. 4.

#### IV. SUMMARY AND CONCLUSION

In the present work, we have investigated the photoproduction of the charged pion with the  $\Delta(1232, 3/2^+)$  baryon off the proton target at tree level, using the effective Lagrangian method beyond the resonance region. We took into account the nucleon- and  $\Delta$ -pole diagrams corresponding to  $s$ - and  $u$ -channel contributions, respectively. The  $\pi$  and  $\rho$  exchanges are considered in the  $t$ -channel. In order for the gauge invariance of the scattering amplitude, the contact-term contribution was further included together with the gauge-invariant scheme for the form factors. The Regge trajectories for the  $\pi$  and  $\rho$  mesons are introduced to describe the high-energy experimental data correctly. We introduced an ansatz designated to interpolate the Feynman and Regge propagators. These three different cases were assigned as the Born, Regge, and interpolation models. It turned out that the present numerical results are in good agreement with the experimental data and could provide useful theoretical guides and estimations for the future experiments. We list the important observations in the present work as follows:

- Unpolarized physical quantities such as the energy and angular dependences of the cross sections are reproduced qualitatively well beyond the resonance region  $E_{\text{cm}} \gtrsim 2$  GeV for the interpolation model, in comparison to the presently available experimental data.
- We observe a strong peak in the forward-scattering region which is suppressed with respect to  $E_\gamma$ . It also turns out that this forward peak is generated by the  $t$ -channel pseudoscalar-meson ( $\pi$ ) exchange on top of the subleading contact-term contribution, although the latter gets stronger as  $E_\gamma$  increases. In general, the peak shifts to the very forward region as  $E_\gamma$  increases.
- The momentum-transfer dependence of the  $d\sigma/dt$  shows that the present framework is not enough to reproduce the experimental data for the region  $E_\gamma \lesssim 3.5$  GeV and  $-t \gtrsim 0.05$  GeV<sup>2</sup>. The observed discrepancy may indicate the necessity of the further unknown contributions from the higher-spin meson exchanges in the  $t$  channel as well as the baryon resonances, which are not taken into account in the present work.
- On the contrary, the present theoretical framework provides a very good agreement with the experimental data for the high-energy region beyond  $E_\gamma \approx 5$  GeV. Especially, the ansatz for the Feynman-Regge interpolation plays an important role to reproduce the data correctly.
- We also present the numerical results for one of the various double polarization observables, i.e., the polarization-transfer coefficients  $C_{x,z}$ . Satisfying the condition of the collinear-limit for  $E_\gamma \gtrsim 8$  GeV, the observable  $C_{x,z}$  remains almost unchanged, whereas nontrivial structures are shown at the forward scattering regions due to the interference between the contact-term and  $\pi$  exchange contributions.
- From the numerical results in the  $\pi^+$  decay-angle distribution function, we find that in the low energy region the spin-1 exchange (small  $\rho$ -meson exchange plus the large contact-term contribution) and that of the spin-0 ( $\pi$ -exchange) competes with each other, depending on the  $\theta$  angles. In contrast, only the spin-1 exchanges, such as the contact-term contribution with the small but finite  $\rho$ -meson exchange give the dominant contribution to the process in the high-energy region, i.e. the contact-term contribution.

In conclusion, the present theoretical framework can reproduce the available experimental data qualitatively well, although other resonances and higher-spin meson exchanges are not considered here. The deviations observed in the region  $E_\gamma \lesssim (3 \sim 4)$  GeV, therefore, could be improved by taking into account those contributions. Especially, it also turns out that the role of the Feynman-Regge interpolation is very crucial to reproduce the experimental data correctly in the higher-energy region. Moreover, being different from the  $\Lambda(1520, 3/2^-)$  photoproduction where the contact-term is dominant, the  $t$ -channel meson exchange and contact-term contributions are competing with each other in the  $\Delta(1232, 3/2^+)$ , especially for the lower-energy region. The results from the present theoretical work would be the

useful guides and estimations for the high-energy photon-beam experiment, such as the future experiments planned in the LEPS2 at SPring-8 and the CLAS12 at the Jefferson laboratory, for instance. More sophisticated works, with other  $\pi\Delta$  isospin-channels, nucleon resonances and other contributions, are under progress and will appear elsewhere.

### Acknowledgment

The authors are grateful to C. W. Kao, A. Hosaka, H.-Ch. Kim for fruitful discussions. This work was supported by the grant NRF-2010-0013279 from National Research Foundation (NRF) of Korea. The numerical calculations were partially performed via SAHO at RCNP, Osaka University, Japan. All the figures in the present work were generated using PLOT [45] and JAXODRAW [46].

- 
- [1] S. i. Nam, A. Hosaka and H. -Ch. Kim, Phys. Rev. D **71**, 114012 (2005).
  - [2] T. Nakano, talk given at the 11th Asia Pacific Physics Conference (APPC11), Shanghai, China.
  - [3] H. Toki, C. Garcia-Recio and J. Nieves, Phys. Rev. D **77**, 034001 (2008).
  - [4] S. i. Nam, Phys. Rev. C **81**, 015201 (2010).
  - [5] S. i. Nam and C. W. Kao, Phys. Rev. C **81**, 055206 (2010).
  - [6] B. G. Yu, T. K. Choi and W. Kim, Phys. Rev. C **83**, 025208 (2011).
  - [7] B. G. Yu, T. K. Choi and W. Kim, arXiv:nucl-th/1104.3672.
  - [8] CLAS12, <http://www.jlab.org/Hall-B/clas12/>
  - [9] LEPS2, <http://www.hadron.jp/>
  - [10] M. Ripani *et al.*, Nucl. Phys. A **672**, 220 (2000).
  - [11] J. C. Nacher and E. Oset, Nucl. Phys. A **674**, 205 (2000).
  - [12] R. B. Clark, Phys. Rev. D **18**, 1444 (1978).
  - [13] G. R. Goldstein and J. F. Owens, Nucl. Phys. B **71**, 461 (1974).
  - [14] W. Rarita and J. Schwinger, Phys. Rev. **60**, 61 (1941).
  - [15] S. Ozaki, H. Nagahiro and A. Hosaka, Phys. Rev. C **81**, 035206 (2010).
  - [16] K. Nakamura [Particle Data Group], J. Phys. G **37**, 075021 (2010).
  - [17] H. -Ch. Kim and M. Praszalowicz, Phys. Lett. B **585**, 99 (2004).
  - [18] G. S. Yang, H. -Ch. Kim, M. Praszalowicz and K. Goetze, Phys. Rev. D **70**, 114002 (2004).
  - [19] M. A. B. Beg, B. W. Lee and A. Pais, Phys. Rev. Lett. **13**, 514 (1964).
  - [20] C. Amsler *et al.* [Particle Data Group], Phys. Lett. B **667** 1 (2008).
  - [21] J. A. Niskanen, Phys. Lett. B **107**, 344 (1981).
  - [22] J. Flender and M. F. Gari, Z. Phys. A **343**, 467 (1992).
  - [23] H. Habermann, C. Bennhold, T. Mart and T. Feuster, Phys. Rev. C **58**, 40 (1998).
  - [24] R. M. Davidson and R. Workman, Phys. Rev. C **63**, 025210 (2001).
  - [25] H. Habermann, K. Nakayama and S. Krewald, Phys. Rev. C **74**, 045202 (2006).
  - [26] T. Regge, Nuovo Cim. **14**, 951 (1959).
  - [27] M. Vanderhaeghen, M. Guidal and J. M. Laget, Phys. Rev. C **57**, 1454 (1998).
  - [28] T. Corthals, J. Ryckebusch and T. Van Cauteren, Phys. Rev. C **73**, 045207 (2006).
  - [29] T. Corthals, D. G. Ireland, T. Van Cauteren and J. Ryckebusch, Phys. Rev. C **75**, 045204 (2007).
  - [30] J. W. C. McNabb *et al.* [The CLAS Collaboration], Phys. Rev. C **69**, 042201 (2004).
  - [31] A. V. Anisovich *et al.*, Eur. Phys. J. A **34**, 243 (2007).
  - [32] D. P. Barber *et al.* [LAMP2 Group], Z. Phys. C **7**, 17 (1980).
  - [33] J. Ballam *et al.*, Phys. Rev. D **5**, 545 (1972).
  - [34] W. Struczinski *et al.*, Nucl. Phys. B **47**, 436 (1972).
  - [35] J. Ballam *et al.*, Phys. Rev. D **7**, 3150 (1973).
  - [36] D. P. Barber *et al.* [LAMP2 Group], Z. Phys. C **6**, 93 (1980).
  - [37] A. Boyarski *et al.*, Phys. Rev. Lett. **22**, 148 (1969).
  - [38] R. L. Anderson *et al.*, Phys. Rev. D **14**, 679 (1976).
  - [39] D. J. Quinn *et al.*, Phys. Rev. D **20**, 1553 (1979).
  - [40] W. Struczinski *et al.* [Aachen-Hamburg-Heidelberg-Munich Collaboration], Nucl. Phys. B **108**, 45 (1976).
  - [41] Brown-Harvard-MIT-Padova-Weizmann Institute Bubble Chamber Group, Phys. Rev. **155**, 1468 (1967).
  - [42] N. Muramatsu *et al.*, Phys. Rev. Lett. **103**, 012001 (2009).
  - [43] K. Schilling, P. Seyboth and G. E. Wolf, Nucl. Phys. B **15**, 397 (1970) [Erratum-ibid. B **18**, 332 (1970)].
  - [44] S. P. Barrow *et al.* [CLAS Collaboration], Phys. Rev. C **64**, 044601 (2001).
  - [45] <http://plot.micw.eu/> (PLOT).
  - [46] <http://jaxodraw.sourceforge.net/> (JAXODRAW).

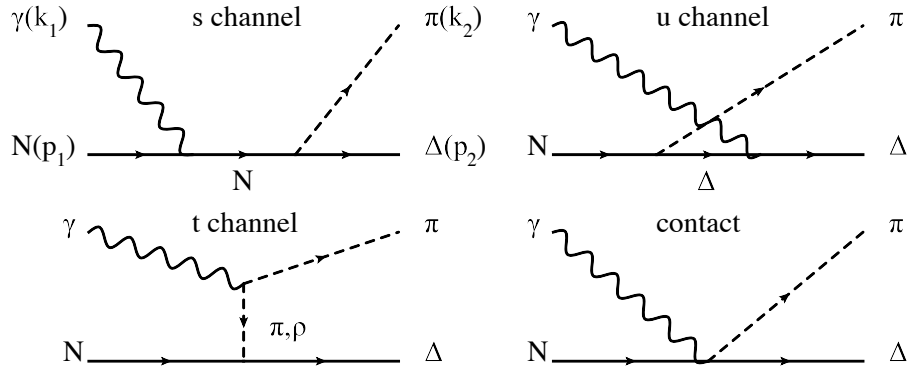


FIG. 1: Relevant Feynman diagrams for the  $\gamma N \rightarrow \pi \Delta(1232)$  reaction process.

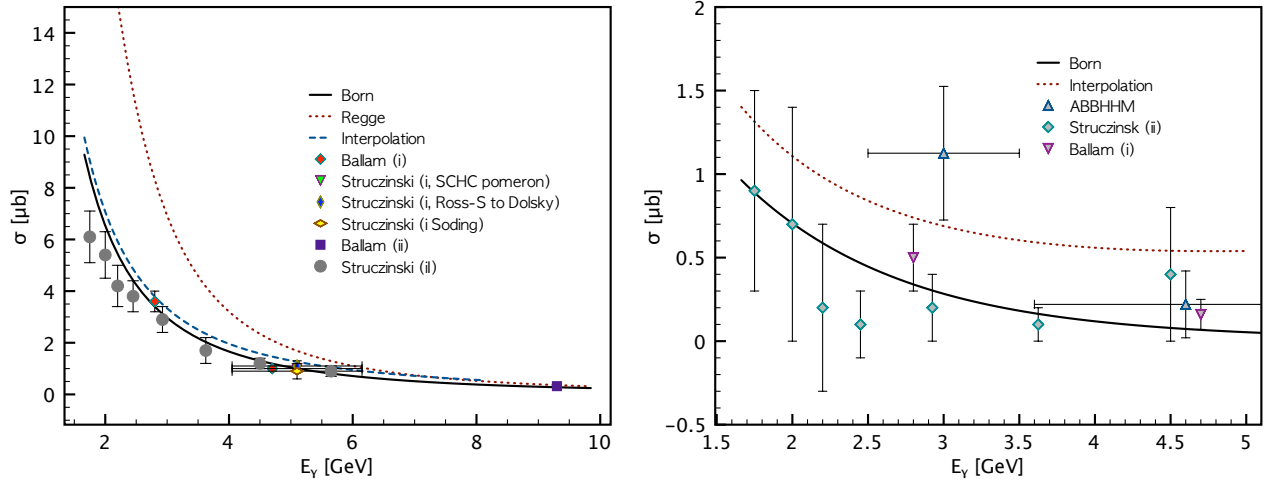


FIG. 2: (Color online) Total cross sections for the  $\gamma p \rightarrow \pi^- \Delta^{++}$  (left) and  $\gamma p \rightarrow \pi^+ \Delta^0$  reaction processes as a function of  $E_\gamma$ . Experimental data are taken from Refs. [33] (Ballam (i)), [34] (Struczinski (i)), [35] (Ballam (ii)), [40] (Struczinski (ii)), and [41] (ABBHHM). We show the curves for the numerical results for the Born terms (solid), that plus the Regge (dot), those with the interpolation (dash), separately. For more details, see the text.

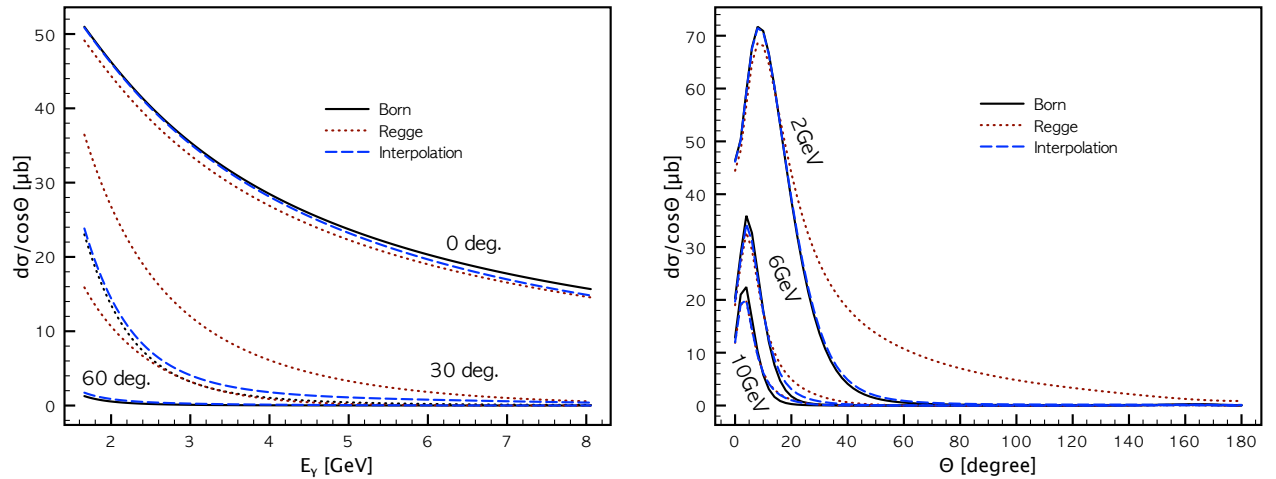


FIG. 3: (Color online) Differential cross section for  $\gamma p \rightarrow \pi^- \Delta^{++}$  as a function of  $E_\gamma$  for different angles  $\theta = (0, 30^\circ, 60^\circ)$  for the Born terms (solid), that plus the Regge (dot), those with the interpolation (dash), separately in the left panel. In the right panel, we plot the differential cross section as a function of  $\theta$  for different energies,  $E_\gamma = (2, 6, 10)$  GeV, represented in the same manner with the left panel.

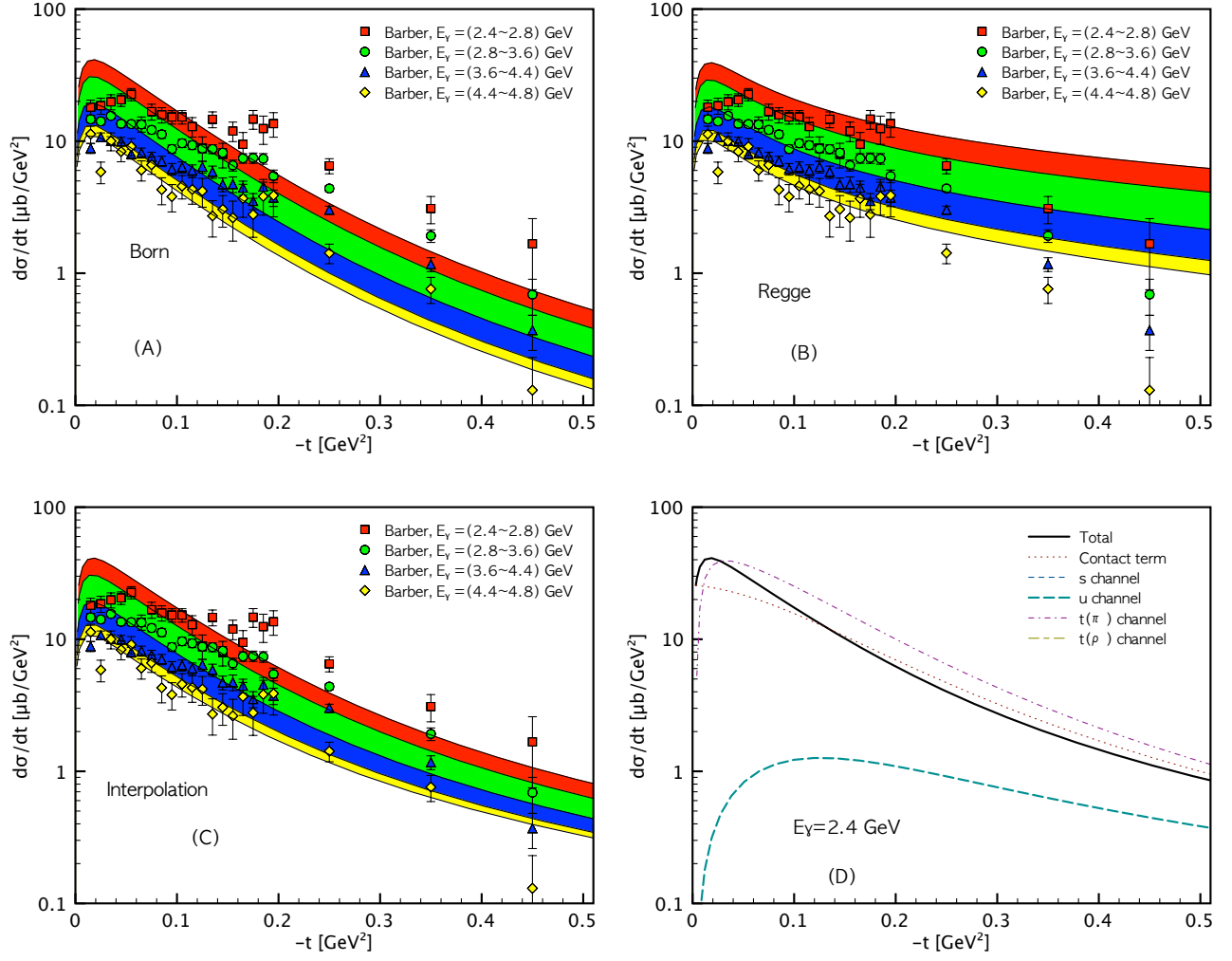


FIG. 4: (Color online) Momentum-transfer dependence  $d\sigma/dt$  [ $\mu\text{b}/\text{GeV}^2$ ] for  $\gamma p \rightarrow \pi^- \Delta^{++}$  as a function of  $-t$  [ $\text{GeV}^2$ ] for the low-energy region  $E_\gamma = (2.4 \sim 4.8)$  GeV for the Born (A), Regge (B), interpolation (C) models, separately. Experimental data are taken from Ref. [36] (Barber). Each contribution is also drawn for  $E_\gamma = 2.4$  GeV for the Born model (D). In the panel (E), we draw the numerical result for the  $\gamma p \rightarrow \pi^+ \Delta^0$ , using only the interpolation model.

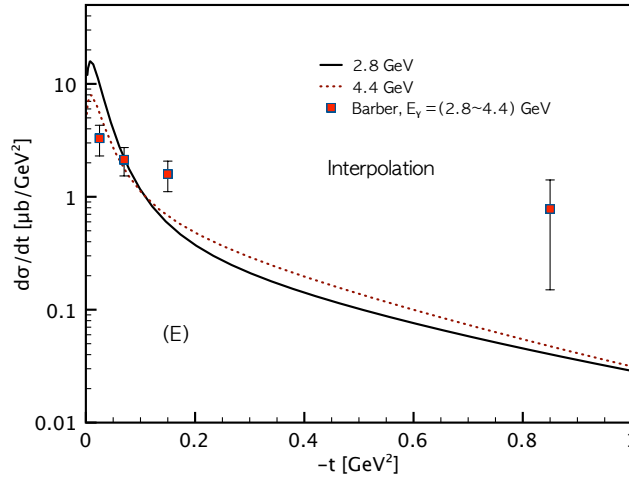


FIG. 5: (Color online) Momentum-transfer dependence  $d\sigma/dt$  [ $\mu\text{b}/\text{GeV}^2$ ] for  $\gamma p \rightarrow \pi^+ \Delta^0$  as a function of  $-t$  [ $\text{GeV}^2$ ] for the low-energy region  $E_\gamma = (2.4 \sim 4.8)$  GeV for the interpolation model. Experimental data are taken from Ref. [36] (Barber).

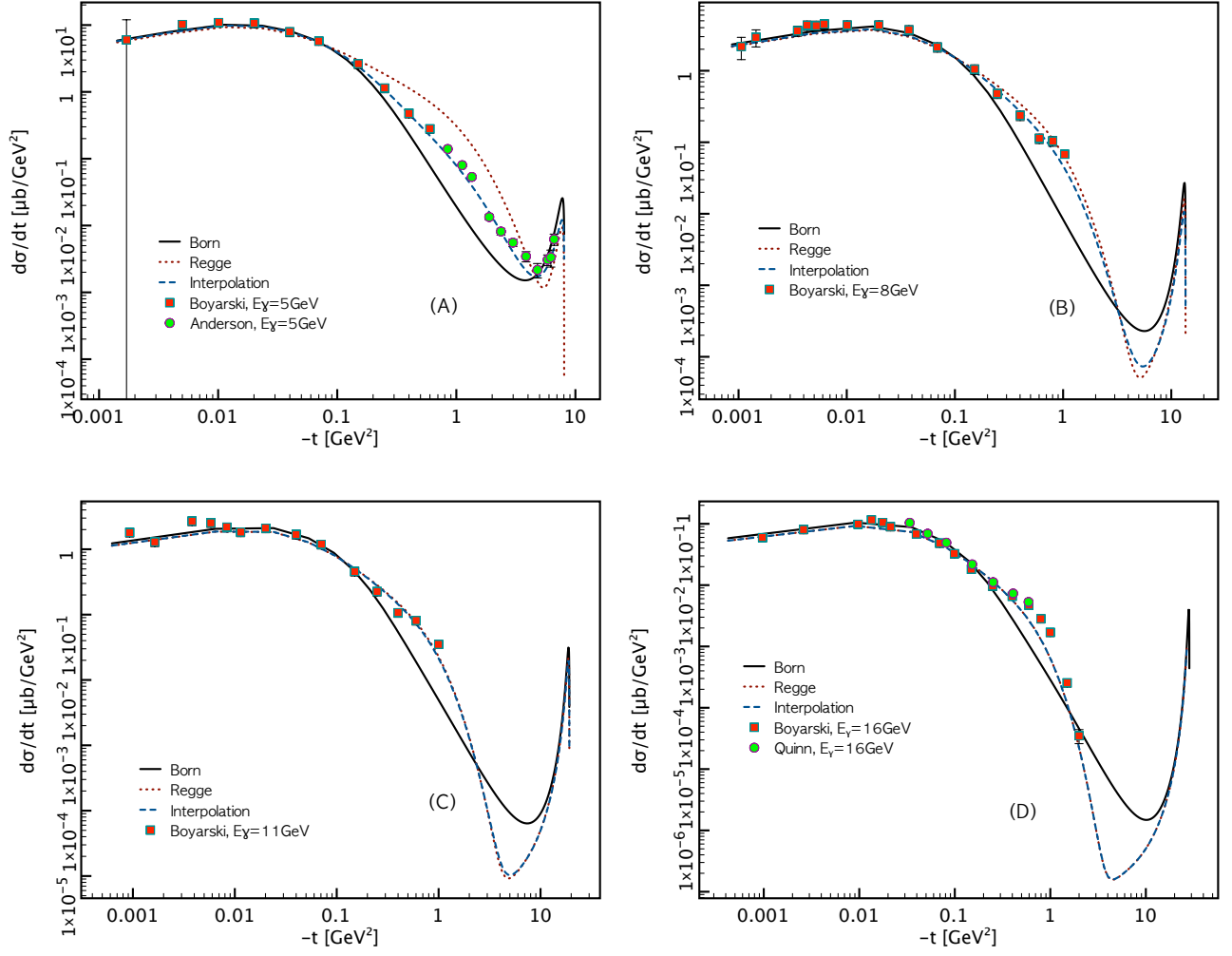


FIG. 6: (Color online) Momentum-transfer dependence  $d\sigma/dt$  [ $\mu\text{b}/\text{GeV}^2$ ] for  $\gamma p \rightarrow \pi^- \Delta^{++}$  as a function of  $-t$  [ $\text{GeV}^2$ ] for the high-energy region  $E_\gamma = (5, 8, 11, 16)$  GeV in panel (A,B,C,D). Experimental data are taken from Refs. [37] (Boyarski), [38] (Anderson), and [39] (Quinn).

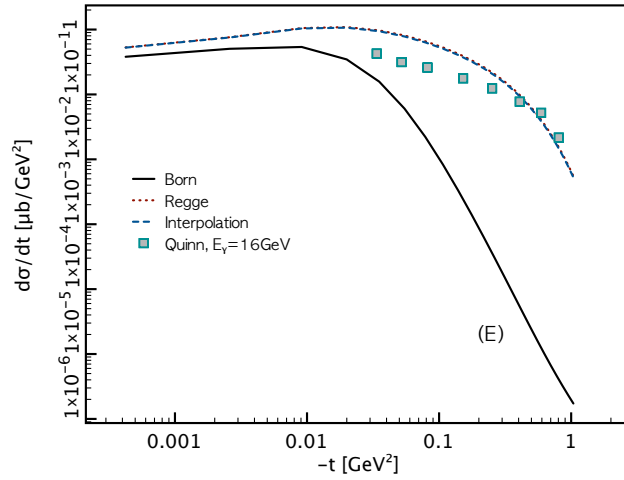


FIG. 7: (Color online) Momentum-transfer dependence  $d\sigma/dt$  [ $\mu\text{b}/\text{GeV}^2$ ] for  $\gamma p \rightarrow \pi^+ \Delta^0$  as a function of  $-t$  [ $\text{GeV}^2$ ] for  $E_\gamma = 16 \text{ GeV}$ . Experimental data are taken from Ref. [39] (Quinn).

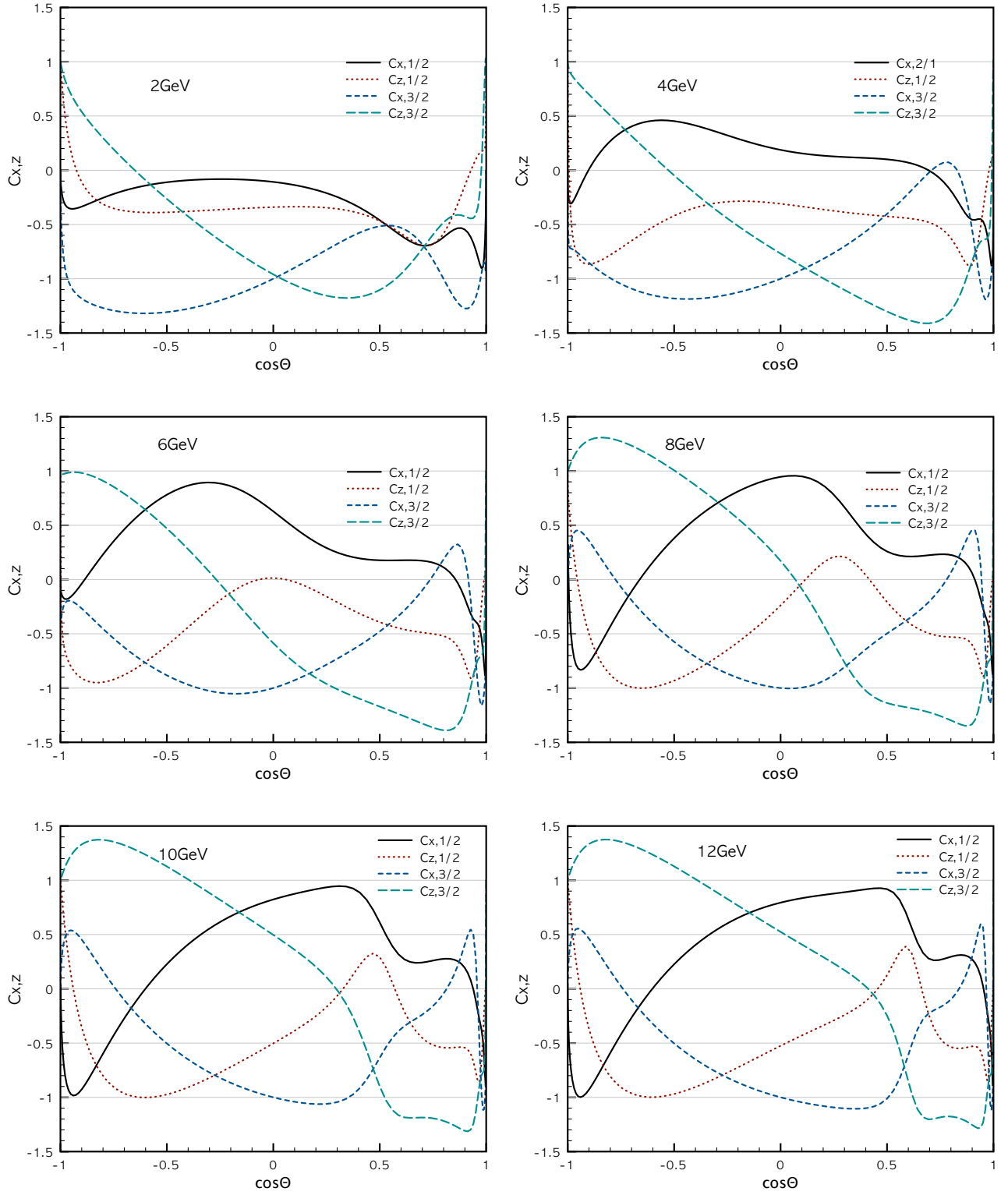


FIG. 8: (Color online) Polarization-transfer coefficients,  $C_{x,z}$  for the spin-1/2 and 3/2 components for  $\gamma p \rightarrow \pi^- \Delta^{++}$  as functions of  $\cos\theta$  for different photon energies,  $E_\gamma = (2, 4, 6, 8, 10, 12)$  GeV, computed from the interpolation model.

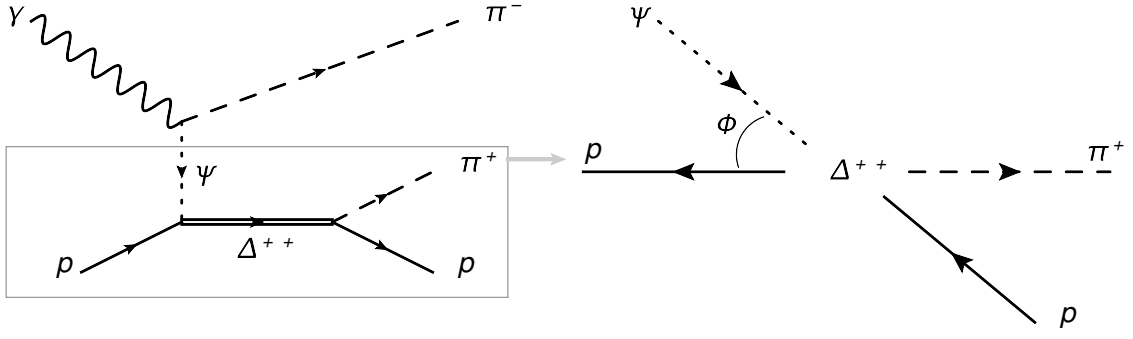


FIG. 9: Feynman diagram for  $\gamma p \rightarrow \pi^+ \pi^- p$  in the left panel. In the box, the subsequent process,  $\psi p \rightarrow \Delta^{++} \rightarrow \pi p$ , is depicted, where  $\psi$  indicates a meson exchanged. The diagram in the box can be interpreted using the Gottfried-Jackson frame as shown in the right panel. The angle  $\phi$  is defined by that between the initial and final particles.

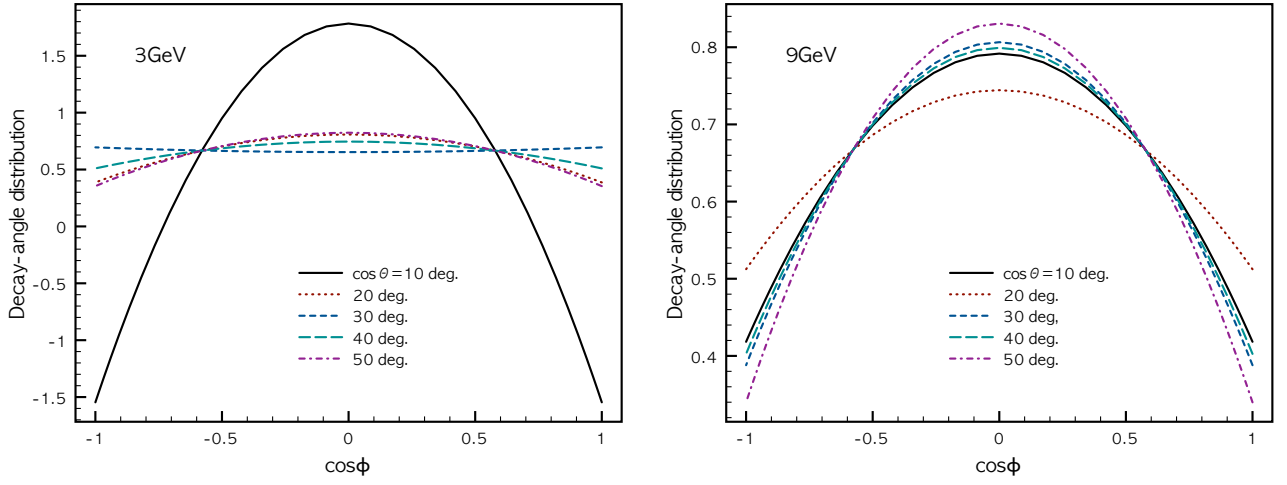


FIG. 10: (Color online)  $\pi^+$  decay-angle distribution for  $\gamma p \rightarrow \pi^- \Delta^{++}$  as a function of  $\cos \phi$ , which is the angle between the  $p$  and  $\pi^+$  decaying from  $t\Delta^{++}$  in the Gottfried-Jackson frame (see Fig. 9), for two different photon energies  $E_\gamma = (3, 9)$  GeV.